

RESEARCH

Open Access



The links between dietary diversity and RNA virus diversity harbored by the great evening bat (*Ia io*)

Zhenglanyi Huang^{1,2}, Zhiqiang Wang^{1,2}, Yingying Liu^{1,2}, Can Ke^{1,2}, Jiang Feng^{1,3*}, Biao He^{4*} and Tinglei Jiang^{1,2*}

Abstract

Background Predator–prey interactions and their dynamic changes provide frequent opportunities for viruses to spread among organisms and thus affect their virus diversity. However, the connections between dietary diversity and virus diversity in predators have seldom been studied. The avivorous bats, *Ia io*, show a seasonal pattern of dietary diversity. Although most of them primarily prey on insects in summer, they mainly prey on nocturnally migrating birds in spring and autumn.

Results In this study, we characterized the RNA virome of three populations of *I. io* in Southwest China during summer and autumn using viral metatranscriptomic sequencing. We also investigated the relationships between dietary diversity and RNA virus diversity by integrating DNA metabarcoding and viral metatranscriptomic sequencing techniques at the population level of *I. io*. We found 55 known genera belonging to 35 known families of RNA viruses. Besides detecting mammal-related viruses, which are the usual concern, we also found a high abundance of insect-related viruses and some bird-related viruses. We found that insect-related viruses were more abundant in summer, while the bird-related viruses were predominantly detected in autumn, which might be caused by the seasonal differences in prey selection by *I. io*. Additionally, a significant positive correlation was identified between prey diversity and total virus diversity. The more similar the prey composition, the more similar the total virus composition and the higher the count of potential new viruses. We also found that the relative abundance of *Picornaviridae* increased with increasing prey diversity and body mass.

Conclusions In this study, significant links were found between RNA virus diversity and dietary diversity of *I. io*. The results implied that dynamic changes in predator–prey interactions may facilitate frequent opportunities for viruses to spread among organisms.

Keywords Bats, *Ia io*, Viral metatranscriptomic sequencing, RNA virus diversity, Dietary diversity, Virus ecology

*Correspondence:

Jiang Feng

fengj@nenu.edu.cn

Biao He

heb-001001@163.com

Tinglei Jiang

jiangtl730@nenu.edu.cn

Full list of author information is available at the end of the article



© The Author(s) 2024. **Open Access** This article is licensed under a Creative Commons Attribution-NonCommercial-NoDerivatives 4.0 International License, which permits any non-commercial use, sharing, distribution and reproduction in any medium or format, as long as you give appropriate credit to the original author(s) and the source, provide a link to the Creative Commons licence, and indicate if you modified the licensed material. You do not have permission under this licence to share adapted material derived from this article or parts of it. The images or other third party material in this article are included in the article's Creative Commons licence, unless indicated otherwise in a credit line to the material. If material is not included in the article's Creative Commons licence and your intended use is not permitted by statutory regulation or exceeds the permitted use, you will need to obtain permission directly from the copyright holder. To view a copy of this licence, visit <http://creativecommons.org/licenses/by-nc-nd/4.0/>.

Background

Coronavirus disease (i.e., COVID-19) and numerous historical outbreaks of emerging infectious diseases (EID) are a significant threat to human health and the economy [1–4]. Nearly 70% of these diseases originate from wildlife [5, 6]. Metagenomic sequencing has revealed high virus diversity in wildlife [7–9], along with spatial–temporal variations and their associations with host phylogeny, traits, and numerous ecological factors [10–16]. Initially, the virus diversity is impacted by host phylogeny, including the species level and broader taxonomic categories (orders or phyla) [10, 11]. A correlation might exist between the body size of wildlife and their virus diversity. For instance, larger body sizes are likely linked to larger home ranges or access to diverse food sources [17, 18], which could expose them to a broader array of viruses [19]. Alternatively, larger body sizes may indicate longer lifespans [20], potentially affecting the virus diversity encountered throughout their lives [12, 19]. Currently, our understanding of ecological factors linked to virus diversity variations primarily comes from species-level analyses. For example, by comparing the variations in virus diversity among species at a large geographical scale and exploring the associated ecological factors, the results revealed that the variations in diversity or prevalence of viruses were influenced mainly by climate change, land use, human activities, and the host dynamics and functional traits [12, 21, 22]. Recently, some studies have explored ecological factors that may influence spatial–temporal variations in virus diversity in wildlife at the population level [13, 14, 23]. These studies showed that the virus diversity is influenced by environmental heterogeneity (e.g., temperature and humidity), age structure (proportion of juveniles), and colony size in wildlife populations [13, 14, 23]. While numerous studies have identified several ecological factors related to virus diversity variations in wildlife [10–14, 22–27], some critical aspects remain largely unexplored.

Interactions between predator and their prey, along with their dynamic changes, offer significant opportunities for the transmission of viruses and variations in their diversity due to the possible acquisition of prey-related viruses by predators from various sources [10]. Nevertheless, research on the relationship between the diet of wildlife and the virus diversity they harbor remains scarce. Few studies have explored the possibility of predators as recipients of viruses and established links between their diet and the variation in virus diversity. For example, a study showed that simian foamy viruses (SFV) are transmitted to wild chimpanzees (*Pantroglyodytes verus*) because they regularly hunt western red colobus monkeys (*Piliocolobus badius*) [28]. Another study showed that prey density may correlate with the virus richness

in the common vampire bat (*Desmodus rotundus*) across sites [13]. Finally, a study revealed that mosquitoes carry several specific RNA viruses and there is a significant co-occurrence relationship between these viruses and their corresponding food sources at the species level [15]. However, these studies focused only on the single virus of a species of interest and the effects of prey density on virus diversity. The connections between dietary diversity and the virus diversity in wildlife should be systematically investigated. In addition to spatial variation among populations, some species show considerable individual and/or temporal dietary variation [29–32], which may also influence the types of viruses they harbor [33]. Thus, changes in the virus communities of predators might be expected when they hunt different prey across various seasons. However, the connections between prey diversity and the virus diversity in wildlife are infrequently examined within a population.

Bats are the second most diverse mammalian order, with more than 1400 species around the world [34]. Many unique biological, ecological, immunological, and genetic characteristics of bats enable them to carry a greater variety of viruses than most other mammals, including several emerging viruses that can cause infectious diseases in humans [16, 35–37]. Virus diversity of bats is associated with variations in ecological factors, including local climate, food resource density, elevation, age structure, genetic distance, and population dynamics [13, 16]. Most bat species mainly feed on arthropods, although some species also expand their diets with small vertebrates, such as fish, frogs, and birds [32]. Among them, avivorous bats are excellent natural models for investigating the links between prey diversity and virus diversity of bat predators at the population level for several reasons. First, avivory in bats implies dietary expansion (from insects to birds) relative to other insectivorous species. Like bats, birds act as hosts for many types of viruses. Thus, when bats eat birds, they also consume the viruses of birds. This may lead to variation in the virus composition of these bats due to the accumulation of viruses with various combinations. Second, three bat species, including *Nyctalus lasiopterus*, *Nyctalus aviator*, and *I. io*, mainly hunt insects in summer, but they mainly hunt nocturnally migrating birds in spring and autumn [32, 38–42]. Our previous studies also revealed that most individuals of *I. io* hunted insects in summer, but 78% of individuals hunted nocturnally migrating birds (at least 22 passerine birds) in autumn [32]. Seasonal variations in dietary and spatial niches at the population and individual levels was also reported in our previous studies [31, 43]. This shift in the diet provides an opportunity to assess the differences in virus communities of predators across seasons, including total virus diversity and

composition. Moreover, the seasonal changes in prey diversity (i.e., insects and birds) of avivorous bats can facilitate the assessment of the relationships between prey diversity and virus diversity in predators.

In this study, three populations of the avivorous bat *I. io* were selected to investigate the links between dietary diversity and RNA virus diversity through conducting DNA metabarcoding sequencing and viral metatranscriptomic analysis. Here, we first hypothesized that there would be a significant link between the RNA virus diversity carried by *I. io* and the prey diversity it preys on. Then, we make three predictions. Firstly, the virus diversity harbored by *I. io* exhibits seasonal variations consistent with dietary diversity, with a higher relative abundance of insect prey and insect-related viruses in summer and bird prey and bird-related viruses in autumn. Secondly, the diversity of virus species would increase with the increase in prey species diversity; as the similarity in prey composition rises, so does the similarity in virus composition. Finally, a positive correlation is expected between the relative abundance of prey and prey-related viruses in *I. io*. Additionally, it was hypothesized that virus species diversity is correlated with the body size of *I. io*. It was predicted that virus species diversity would increase with an increase in body mass in *I. io*.

Materials and methods

Sample collection and morphological measurements

We captured *I. io* using a mist net at cave entrances when bats returned from their foraging sites before sunrise. Feces, oral, and anal swabs of seemingly asymptomatic individuals were separately obtained from three locations in Southwest China, including Xingyi City, Guizhou Province (abbreviation: XY), Kaili City, Guizhou Province (abbreviation: KL), and Weishan County, Yunnan Province (abbreviation: WS), in the summer (June–July) and autumn (September–December) of 2021. Each bat was placed in a clean and sterilized paper bag until they defecated (less than 2 h). Fecal pellets were collected from the sterile paper bags and stored in 2 mL freeze-storage tubes (Corning, USA). Two fecal samples were collected from each individual for viral metatranscriptomic sequencing and DNA metabarcoding sequencing, respectively. After each bat defecated, we recorded their body mass using an electronic balance (ProScale LC-50, Accurate Technology, Inc., Asheville, NC, USA) to the nearest 0.01 g and their forearm length using a digital caliper (TESA-CAL IP67, Tesa Technology, Renens, Switzerland) to the nearest 0.01 mm. In this case, the body mass of the bats was not affected by their physiological condition (i.e., satiation level). We used flocking swabs to collect oral and anal swab samples after recording the parameters above. The swab samples were also stored in 2 mL freeze-storage

tubes (Corning, USA). We marked individuals by cutting their hair on the back to avoid collecting data from the same individual. We collected samples at approximately two-day intervals to avoid the negative effects of capturing bats every day. Sample collection was performed at least thrice at each sampling location in each season to collect enough samples. We released the bats in their habitat after sampling. Each sample was frozen in liquid nitrogen immediately after collection. After all samples were collected, we transported them to the laboratory with dry ice and stored them at -80°C until use.

Viral metagenomic sequencing and analysis

Sample pre-treatment

First, we combined the samples collected at each sampling location during every season to obtain three pooled samples. Each pooled sample comprised fecal and corresponding swab samples from 5 to 10 distinct bat individuals. In total 18 pooled samples were obtained with half in the summer group and the other half in the autumn group. Each pooled sample was labeled on the basis of the “sampling location, sampling season, and sample number,” such as “XYsu1”. Before the nucleic acid and library construction, each pooled sample was pretreated as follows. First, eight volumes (w/v) of precooled sterile SB buffer and zirconium beads were added to every pooled sample and vortexed for 5 min using a vortex oscillator (ST-0246, USA SI). Then, the treatment solution was frozen and thawed thrice to ensure adequate cell lysis. We centrifuged the treatment solution at $12,000\times g$ for 5 min at normal atmospheric temperature ($20 - 25^{\circ}\text{C}$) using a Thermo Legend Micro 21 centrifuge (Thermo) and collected the supernatant. Cell fragments and bacteria in the supernatant were removed using a $0.45\ \mu\text{m} + 0.22\ \mu\text{m}$ filter membrane (JET BIOFIL). Then, 1 mL of the filtrate was transferred into an ultracentrifuge tube containing 28% (w/w) sucrose, and centrifuged at $160,000\times g$ for 2 h at 4°C using a HIMAC CP 100wx ultracentrifuge (Hitachi, Tokyo, Japan). After removing the supernatant, the pellet was resuspended in 200 μL of SB buffer. Then, EMB and EM were added proportionally to the resuspension, which was then incubated at 37°C for 60 min to remove free DNA. We added 2 μL of SS to the DNA-free resuspension and mixed it well to deactivate the DNA enzyme for 10 min at $65 - 75^{\circ}\text{C}$. Then, the DNA-free resuspension was centrifuged at 2000 rpm for 5 min at room temperature. Finally, 200 μL of the supernatant was stored at -20°C for subsequent experiments.

Extraction and quality inspection of nucleic acid

We co-extracted DNA and RNA from the above 200 μL supernatant using TaKaRa MiniBEST Viral RNA/DNA Extraction Kit Ver.5.0 (Takara, Japan). Then, a DNA

digestion enzyme was used to digest the DNA in the total nucleic acid. The remaining whole transcriptome was amplified using the 150,054 REPLI-g Cell WGA & WTA Kit (Qiagen, Germany). Finally, the quality of the amplified products was evaluated using NanoDropOne (Thermo Scientific, USA), Qubit 4.0 (Life Technologies, USA), and 1.5% agarose gel electrophoresis before library construction and sequencing. All amplified products were stored at -80°C until the library was constructed.

Library preparation and sequencing

The ALFA-SEQ DNA Library Prep Kit (Finorop, China) was used for library preparation. The quantity and quality of the libraries were assessed based on the Qubit[®] dsDNA HS Assay Kit (Life Technologies, Grand Island, NY) and the Agilent 4200 System (Agilent, Santa Clara, CA). Finally, paired-end (150 bp reads) sequencing for each library was performed on the Illumina Novaseq 6000 platform by Magigene.

Raw data preprocessing and virus identification

The quality of the raw reads of each library was first checked using FastQC version 0.11.7 [44] and trimmed using Trimmomatic version 0.38 [45] to obtain clean reads. Then, the reads of the host genome in the clean reads were removed using Bowtie2 version 2.4.1 [46]. We used the highly sensitive end-to-end mode to compare clean reads of every library to the genome assembly of *I. io* (GenBank accession no. GCA_025583905.1). Then, we removed the successfully aligned reads from the library. Fast taxonomic classification of bacteria, archaea, and fungi of the remaining reads was performed using Kraken2 version 2.0.9b [47] with a custom RefSeq-based database. Unclassified reads of each library were assembled de novo using MEGAHIT version 1.1.3 [48] to get contigs. Contigs ≥ 500 bp were retained for annotation. Briefly, all retained contigs were first compared to the EVRD [49] using BLASTn version 2.7.1 and DIAMOND version 0.9.25 [50] with an *e*-value threshold of 1×10^{-5} . Then, the BLASTn-classified and DIAMOND-classified sequences were defined in the final viral contigs assemblage if they met the following criteria. First, these sequences did not match the false reference sequences identified in our refined EVRD-nt and EVRD-aa reference databases; the sequences may be contaminants related to host genomes, laboratory components, nonviral organisms, or artifacts [51]. Second, these sequences had no significant hits to non-virus nt and nr databases by BLASTn/x ($e \geq 1e^{-20}$ and identity $\leq 50\%$) [52]. Finally, we compared each alternative sequence to a non-redundant nt/nr database for online validation by BLASTn/x. The sequences were considered to be virus contigs if

they had the best hits with amino acids or nucleotide sequences of viruses.

Clustering of non-redundant virus contigs and abundance statistics of virus cluster

The virus contigs were clustered based on the following conditions to obtain non-redundant virus contigs: (1) nucleotide similarity $> 99\%$ among contigs; (2) nucleotide coverage $> 90\%$ among contigs. The genus is a compromising analytic level that can ensure the support of biologically and/or ecologically meaningful virological conclusions [53]. Therefore, non-redundant virus contigs were clustered based on 90% nucleotide identity and 80% nucleotide coverage [53]. Then, the optimal BLASTx hit and classified information of every cluster was obtained based on the virus nt/nr reference database. We argued that the term “host” cannot fully explain the role of bats and other organisms associated with such diverse viruses but that “carrier” is more appropriate to refer to the potential source of detected viruses from bats. We obtained the carrier information of invertebrate-related viruses based on ICTV [54] and NCBI [55] and confirmed the carrier information according to the reference virus sequence reported in other studies. The same methods were also used to preliminarily determine the bird-related viruses. The number of viruses present in bat and bird hosts is increasing. To determine the carrier information of bird-related viruses without confusing them with bat-associated viruses, we constructed phylogenetic trees based on the contigs defined as RdRp. Briefly, we chose the longest sequence available to represent the approximately complete amino acid sequence of the RdRp protein. Then, these sequences were compared to those from the NCBI database [56] using blastx to select the reference sequences. We selected several representative viruses from the genera that were distantly related to our sequences in the same families. The virus sequences were then aligned using MAFFT version 7.48 [57]. We used IQ-TREE version 2.0 [58] and selected the -sc option to shear the ambiguous alignment region to ensure that the results were more accurate. Phylogenetic trees were then constructed using the maximum likelihood (ML) approach implemented in IQ-TREE version 2.0 [58]. We used the TESTMERGE method to select the best amino acid substitution model. This method can compare the performance of multiple models for model selection to optimize the accuracy of the phylogenetic tree. Finally, we used FigTree v1.4.3 [59] to visualize the phylogenetic tree.

To quantify the abundance of virus clusters, we first mapped clean reads back to the above virus clusters to get the read count. We excluded clusters with fewer than 10 reads to reduce false positives [60]. Then, we

calculated the relative abundance of each cluster as the number of viruses reads per million from the total reads in each library (RPM). We conducted RT-PCR validation assays to eliminate false positives due to assembly errors. Briefly, virus contigs representing 11 species were randomly selected to design nested primers (Additional file 1: Table S1). Then, we performed nested RT-PCR (reverse transcription PCR) to obtain the positive rate of each virus in each library. Finally, the reliability of the viral metatranscriptomic sequencing results was verified based on the *Pearson* correlation ($r=0.83 - 1.0$, $P<0.05$; Additional file 2: Figure S1A) between the positive rate and the relative abundance of each virus.

Determining the overview of the virome

To determine the distribution of viruses in the samples, we first visualized the relative abundance of each virus family in each sample by constructing a stacked bar plot. Then, an UpSet plot was used to visualize the distribution of virus clusters among samples. We also showed the relative abundance of virus clusters from different carriers in each sample with a heatmap constructed using the function *pheatmap* in R [61]. All data were visualized using the *ggplot2* package [62].

Dietary metagenomic sequencing and analysis

DNA extraction, PCR amplification, and sequencing

Fecal pellets (150 mg) of every individual were homogenized using a grinder (TL2010S, DHS Life Science & Technology Co., Ltd., Beijing, China) before extraction. Then, total DNA was extracted using a QIAamp® DNA Stool Mini Kit (QIAGEN Canada, Mississauga, ON, Canada) following the manufacturer's protocol. The content and quality of the extracts were assessed using a NanoDrop 2000 UV-vis spectrophotometer (Thermo Fisher Scientific, Wilmington, DE, USA). We used universal primer sets to amplify a cytochrome oxidase I (COI) marker [63]. The primer sets were LCO-1490 (5'-GGTCA ACAATCATAAAGATATTGG-3') [64] and ZBJ-ArtR2c (5'-WACTAATCAATTWCCAAATCCTCC-3') [65, 66]. PCR amplification, purification of amplified products, and library construction were performed following previously described methods [67]. Finally, we performed next-generation sequencing (2×300 bp paired-ends) on the Illumina MiSeq platform (Illumina) following the standard protocols described by Majorbio BioPharm Technology Co., Ltd.

Sequence analysis and taxonomic identification

The paired-end reads in each library were first quality-filtered and assembled using Trimmomatic [45] and FLASH [68]. The DNA sequences were clustered into operational taxonomic units (OTUs) based on 97% identity following

previously described methods [63]. Taxonomic identification was performed by aligning the representative sequence from each OTU to reference sequences in the GenBank [56] and Barcode of Life databases [69]. Orders and families were assigned at >95% and >96.5% identity values, respectively [63]. We classified sequences at the species level when the identity was >98% between the query and the reference sequences [63].

Analysis of variations in virus diversity between seasons

We investigated the temporal variations in virus diversity of *I. io*. First, we estimated the Shannon diversity indices (alpha diversity) of each library using the *vegan* package [70]. Hutcheson's *t*-test was performed to evaluate significant differences in Shannon diversity indices between seasons. Briefly, Hutcheson's *t*-test was conducted separately for samples from each sampling location to control for the potential impact of sampling location on the results. Seasonal variation in Shannon indices was assessed for each biological replicate sample within each sampling location using Hutcheson's *t*-test. Hutcheson's *t*-test was performed three times at each sampling location. Second, we assessed the significant differences in the composition of viruses (beta diversity) between seasons. Briefly, we first calculated Bray-Curtis distances between samples using the *vegdist* function in the *vegan* package [70]. Next, we used the Non-metric Multidimensional Scaling (NMDS) technique to illustrate the differences in virus composition using the *metaMDS* function in the *vegan* package [70]. Then, significant seasonal differences in the virus composition were tested by permutational multivariate analysis of variance (PERMANOVA, 9999 permutations) using the *vegan* package [70]. Then, in order to verify whether the significant seasonal differences in virus composition were affected by the sample dispersion within groups, we tested the significance of sample dispersion within the season using the *Betadisper* function in the *vegan* package [70]. Meanwhile, we also examined whether the differences between seasons were significantly larger than the differences within each season by performing ANOSIM (analysis of similarities) using the *vegan* package [70]. Furthermore, PERMANOVA analysis was conducted using the *adonis2()* function with sampling location as a blocking factor, to examine seasonal variations in virus composition while accounting for the potential impact of sampling location.

We performed the Linear Discriminant Analysis Effect Size (LEfSe) analysis to identify biomarkers with significant seasonal differences. First, we performed Student's *t*-tests and Mann-Whitney *U* tests using the *onewaytests* package [71] to detect virus clusters with a significant difference in relative abundance between seasons. Second, we performed Wilcoxon rank sum tests using

the *onewaytests* package [71] to determine the differences between seasons and corrected through FDR [72]. Finally, we performed a linear discriminant analysis (LDA) to evaluate the viruses with significant seasonal differences ($|\text{LDA score (log)}| > 2$) and obtained the biomarkers between seasons using the *MASS* package [73]. The relative abundance of each biomarker was shown in a heatmap plotted using the *heatmap* package [61]. Virus clusters associated with carriers indicated by biomarkers were selected, and *t*-tests were performed to evaluate seasonal differences in the relative abundance of these viruses using the *onewaytests* package [71].

We used the bipartite network implemented by the *igraph* package [74] to visualize the co-occurrence patterns of prey and mammal-related virus species during summer and autumn. The presence of a virus was postulated when any of the following criteria were fulfilled. (1) A certain virus was represented by more than two virus clusters with RPM values exceeding 10. (2) A certain virus was represented by two virus clusters with RPM values exceeding 10, and one of these virus clusters was identified as the RdRp gene. (3) A certain virus was represented by one virus cluster with RPM values exceeding 10 and was identified as RdRp gene. We also selected genera containing multiple virus species, such as *Arlivirus*, *Cripavirus*, *Sobemovirus*, *Sopolyxivirus*, and investigated the phylogenetic relationships among virus species within these genera using phylogenetic trees based on a partial amino acid sequence of the RdRp protein. The specific methods used were as described previously.

Analysis of variation in prey diversity and body mass between seasons

We investigated the seasonal variation in prey diversity and body size of *I. io*. First, the Shannon diversity index, calculated based on the sequencing results of each library, was used as a metric to quantify prey diversity. The Shannon diversity indices were estimated at the species level of the prey using the *vegan* package [70]. Next, we determined differences in the Shannon indices between seasons by conducting Mann–Whitney *U* tests using the *onewaytests* package [71]. Second, we calculated Bray–Curtis distances between samples using the *vegdist* function in the *vegan* package [70]. We also constructed NMDS plots to display the differences in dietary composition between seasons based on the calculated Bray–Curtis distances using the *metaMDS* function in the *vegan* package [70]. Then, we determined the differences in beta diversity of diet by performing permutational multivariate analysis of variance (PERMANOVA) using the *vegan* package [70].

The differences in body mass between seasons were tested by conducting Mann–Whitney *U* tests using the *onewaytests* package [71].

Analysis of the links between prey diversity, body mass, and virus diversity

To investigate the links between prey diversity (Shannon diversity indices calculated on the basis of prey detected across all libraries), body mass, and total virus diversity, we first constructed a linear model (LM) via the *lm* function in the *MASS* package [73]. Total virus diversity was used as the response variable in the model, with three factors—prey diversity, body mass, and sampling location—as explanatory variables. We initially constructed the full model via the *lm* () function and subsequently employed AICc for model selection using the *dredge* () function in *MuMIn* package [75]. During the process of model selection, if there exists one model with $\Delta\text{AICc} < 2$, then this model will be regarded as our optimal model. However, if there are two or more models with $\Delta\text{AICc} < 2$, we employ the *model.avg* () function in the *MuMIn* package [75] to conduct model averaging. The candidate models, including the null model, are presented in Additional file 3 (Table S2). Then, the variance inflation factor (VIF) was calculated between the predictor variables, revealing a VIF of < 5 , which indicated that no multicollinearity was present among the predictor variables in these optimal models. Finally, we presented the results of these optimal models by constructing forest plots using the *forestplot* package [76]. The Mantel test was performed using the *vegan* package [70] to determine the influence of prey composition on the total virus composition.

Virus species with amino acid identity $< 90\%$ in the hallmark gene (RdRp) of the RNA virus were regarded as potential new viruses [16]. We counted the number of potential new viruses in each sample and assessed the effect of body mass and prey diversity on the number of potential new viruses. First, we used the LM model where the number of potential new viruses (transformed by \log_{10}) was the response variable, and two factors were explanatory variables, including prey diversity and body mass. The same methods of model selection (Additional file 4: Table S3) and visualization were subsequently employed, following the approach used in the total virus diversity model. The Mantel test was conducted using the *vegan* package [70] to determine the influence of prey composition on the number of potential new viruses.

Analysis of the relationships between body mass, prey diversity, prey abundance, and the relative abundance of viruses

To explore the links between body mass, prey diversity, prey abundance, and the relative abundance of viruses, an

LM was constructed with the relative abundance of prey-related viruses (including insect-related and bird-related viruses) as the response variable, and five factors—relative abundance of insect prey, relative abundance of bird prey, prey diversity, body mass, and sampling location—as explanatory variables. We used the same methods as the total virus diversity for selecting (Additional file 5: Table S4) and visualizing this model. Additionally, we used linear regression to evaluate the relationships between the relative abundance of prey and prey-related viruses. An LM was also developed using the relative abundance of *Picornaviridae*, *Coronaviridae*, and *Ia io* picornavirus 1 (a biomarker in mammal-related viruses) as the response variable, and five factors—relative abundance of insect prey, relative abundance of bird prey, prey diversity, body mass, and sampling location—as explanatory variables. The same method was used for model selection (Additional file 6: Table S5–Additional file 8: Table S7) and visualization as that used for assessing total virus diversity.

Before constructing the LMs, attempts were made to build the LMMs using the AICc method with the sampling location as a random effect. The same model selection methods (Additional file 3–8: Table S2–S7) were then used. A comparison of AICc values and *P*-values between LMMs and LMs was conducted to ensure robustness. Similar results were observed for LMs and LMMs, with all LMs showing lower AICc values. Thus, the results of all LMs are presented in the main text, while detailed results of LMMs are available in Additional file 9: Table S8.

In this study, all statistical analyses were performed in R 4.2.2 [77]. All data were visualized using the *ggplot2* package [62] unless stated otherwise.

Results

Overview of the virome

In this study, feces, oral, and anal swabs of *I. io* were collected from 130 seemingly asymptomatic individuals from three locations in Southwest China (Fig. 1;

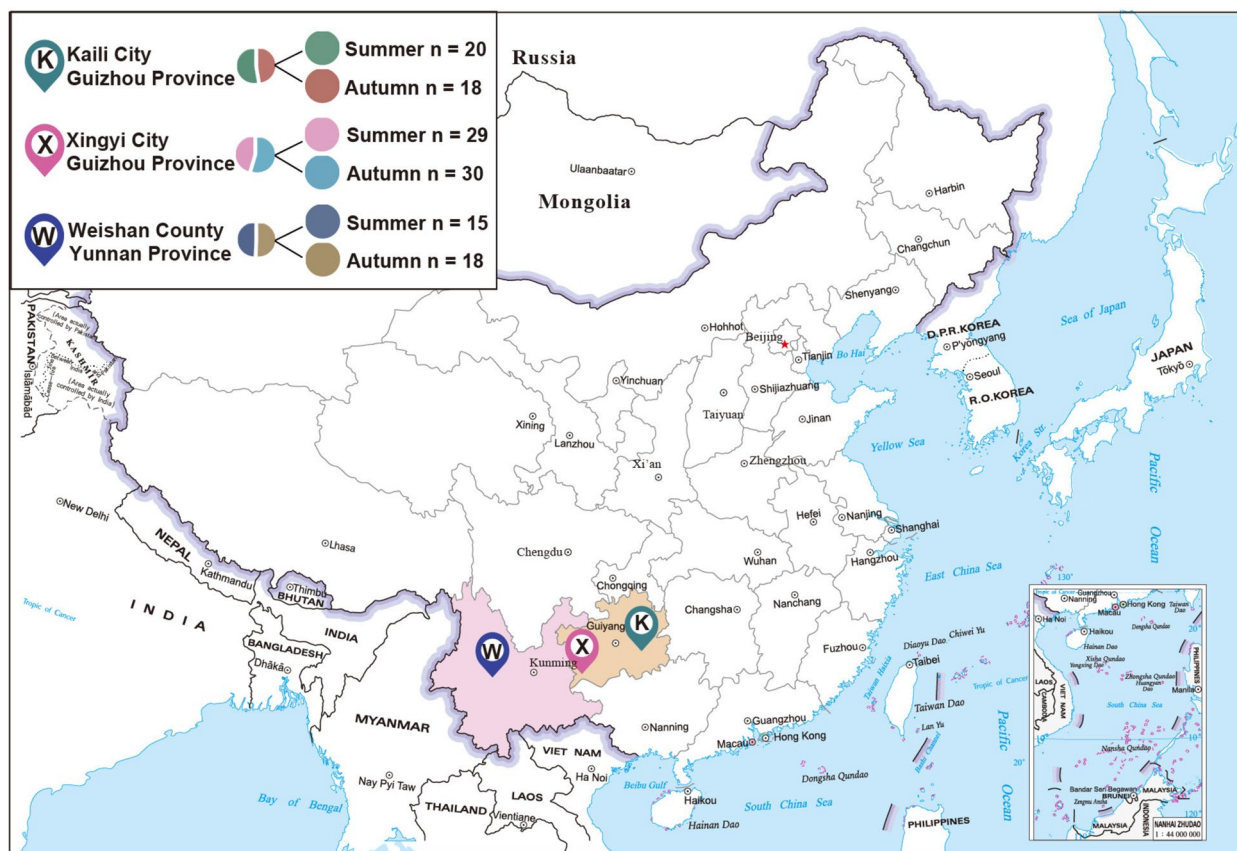


Fig. 1 Overview of the samples used in this study. The sampling was conducted in Yunnan and Guizhou provinces of China, where feces and swab samples were collected. Inset (top-left): The details of the three sampling locations; circles in different colors represent different seasons in each sampling location. The pie chart shows the proportion of bats in each season at each sampling location; “n” represents the number of bats caught in each season at the corresponding sampling location

Additional file 10: Table S9). The 130 individual bats consisted of approximately 60% males and 40% females. In total, feces, oral swabs, and anal swabs from 64 individual bats were collected from June to July (XY: $n=29$; KL: $n=20$; WS: $n=15$), while feces, oral swabs, and anal swabs from 66 individual bats were collected from September to December (XY: $n=30$; KL: $n=18$; WS: $n=18$) (Fig. 1; Additional file 10: Table S9). We obtained 18 libraries following the method to establish libraries described in the Methods section (Additional file 10: Table S9).

In total, 970,272,265 raw reads (291GB) were obtained from the 18 libraries by viral metatranscriptomic sequencing (Additional file 11: Figure S2). At least 10GB of raw reads were obtained from each library (Additional file 11: Figure S2). Among the raw reads, 629,069,342 clean reads remained after the quality check. A total of 92,281 contigs were output by de novo assembly. Contigs longer than 500 bp were retained and used for reference-based annotation (EVRD) after removing redundancy. In total, 4377 clusters were finally obtained after clustering contigs based on 90% nucleotide identity and 80% nucleotide coverage (Additional file 12: Table S10). We randomly selected 11 contigs representing 11 virus species to verify the sequencing results of viral metatranscriptomic sequencing by RT-PCR (Additional file 2: Figure S1B; Additional file 1: Table S1). We found a significant and positive correlation between the positive rate of these viruses and their corresponding relative abundance detected by viral metatranscriptomic sequencing in each sample ($r=0.83-1.0$, $P<0.05$; Additional file 2: Figure S1A). Thus, the RT-PCR analysis confirmed that the results of viral metatranscriptomic sequencing can approximately represent the reality of the virus carried by *I. io*. The annotation was performed for 4377 clusters, which corresponded to 55 known genera of 35 known families of RNA viruses, excluding viruses of unknown classification (Fig. 2A; Additional file 12: Table S10). Among them, most virus clusters were from *Polycipiviridae*, *Picornaviridae*, *Dicistroviridae*, *Solemoviridae*, *Coronaviridae*, *Permutotetraviridae*, *Iflaviridae*, and *Alphatetraviridae* (number of virus clusters: 100 – 365; Fig. 2A; Additional file 12: Table S10).

We found that these virus clusters were associated with various carriers, including insects, mammals, birds, plants, blood-sucking arthropods, etc. (Fig. 2B). Thus, besides detecting mammal-related viruses, we found a high abundance of insect-related and plant-related viruses (Fig. 2B). We also found various bird-related viruses in *I. io*. The results of a phylogenetic analysis based on the partial amino acid sequence of the RdRp protein of *Caliciviridae* showed that our sequences clustered with caliciviruses from birds in several clades,

including Ruddy turnstone calicivirus, Goose calicivirus, Temminck's stint calicivirus, Trumpeter swan calicivirus, Grey teal calicivirus, Duck calicivirus 2, Chicken calicivirus, Ruddy turnstone calicivirus B, Turkey calicivirus, Duck calicivirus 2, Pink-eared duck calicivirus, Ruddy turnstone calicivirus A, and members of *Caliciviridae* in wild birds (Additional file 13: Figure S3). The results of a phylogenetic analysis based on the partial amino acid sequence of the RdRp protein of *Astroviridae* indicated that our sequences clustered with bird-related astroviruses in several clades and formed sister lineages of Turkey astrovirus, *Chicken astrovirus*, Avian astrovirus, Duck astrovirus, Passerine astrovirus in birds, and *Astroviridae* sp. from wild birds (Additional file 14: Figure S4). Finally, the results of a phylogenetic analysis of *Picornaviridae* using the partial amino acid sequence of the RdRp protein showed that our sequences were closely related to *Duck hepatitis A virus*, *Avihepatovirus A*, Blackbird arilivirus, and *Picornaviridae* sp. from birds (Additional file 15: Figure S5).

Seasonal differences in virus diversity

The differences in the relative abundance of virus families between seasons are presented in the stacked plot (Fig. 2A). Virus clusters of *Polycipiviridae*, *Permutotetraviridae*, and *Alphatetraviridae* were predominantly present in samples from summer, while *Picornaviridae* was predominantly present in autumn (Fig. 2A; Additional file 12: Table S10). *Solemoviridae* and *Iflaviridae* were present in samples from both seasons (Fig. 2A; Additional file 12: Table S10). Viruses from the family *Coronaviridae* were found to be more prevalent in samples collected during the summer (Fig. 2A; $t = -4.75$, $P = 4.393e^{-06}$, Fig. 2H; Additional file 12: Table S10). The heatmap also showed differences in the relative abundance of viruses between seasons when we grouped virus clusters according to their carriers (Fig. 2B). For example, a higher relative abundance of insect-related and plant-related viruses was detected in summer (Fig. 2B). These virus contigs represented a variety of virus species from known virus families. Among these, various virus species in each genus, such as *Arlivirus*, *Cripavirus*, *Sobemovirus*, and *Sopolycivirus*, are closely related to each other (Fig. 3). However, a higher relative abundance of various bird-related viruses was mainly detected in autumn (Fig. 2B). We also found that the number of clusters shared between seasons was lower than the number of clusters unique to each season (Fig. 2C). The number of virus clusters unique to samples accounted for about 61.32% of the total virus clusters, whereas the number of virus clusters shared between samples accounted for about 38.68% of the total virus clusters (Fig. 2C). Among the virus clusters unique to samples, about 83.68% were present in summer, and

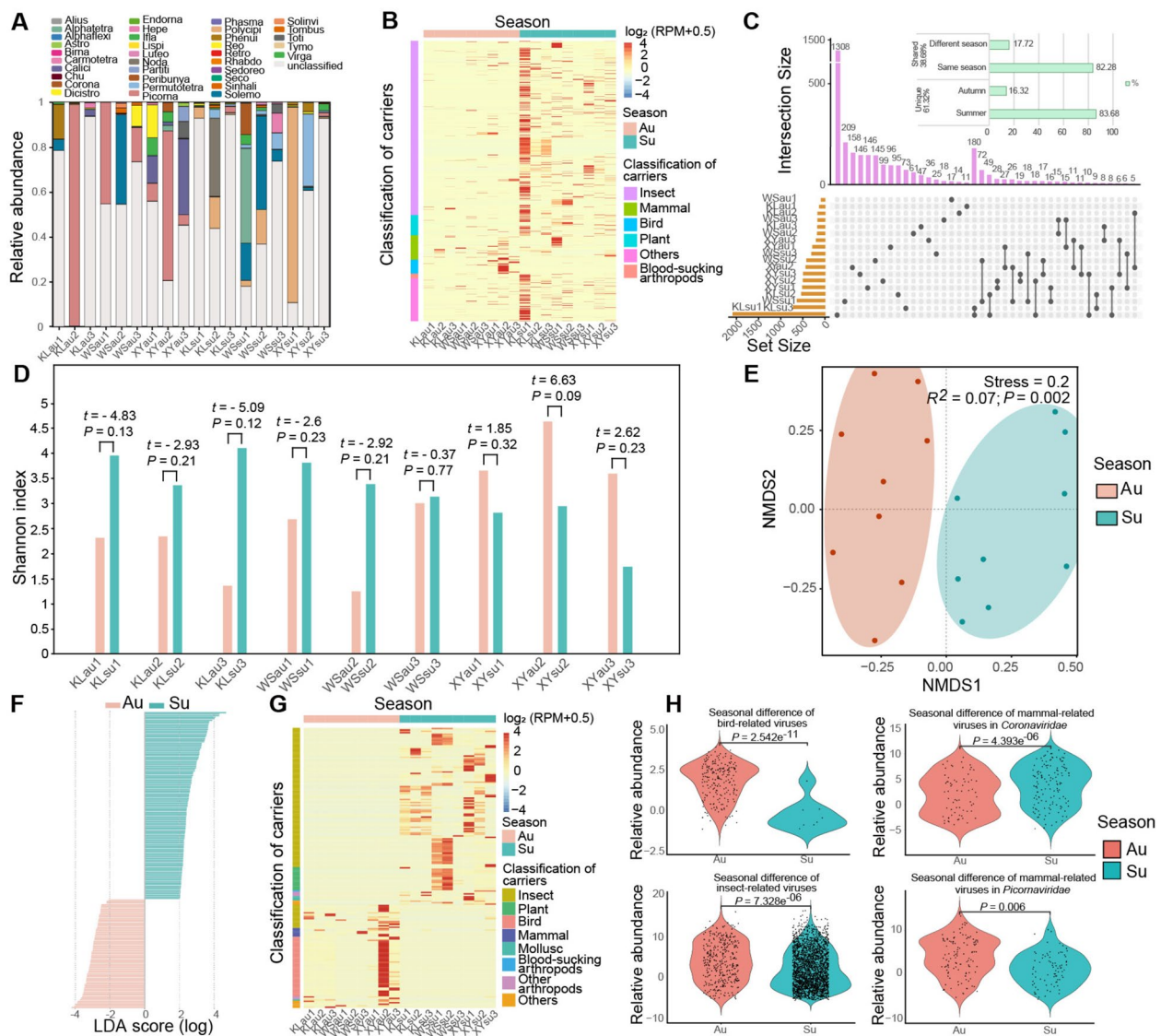


Fig. 2 Overview and seasonal variation of the virome in *I. io*. **A** The stacked bar chart shows the relative abundance of virus families as a proportion of each sample. Different colors represent different virus families. **B** The heat map shows the relative abundance of each carrier-related virus in each sample. The relative abundance of each virus cluster was calculated as $\log_2(\text{RPM} + 0.5)$ to balance the differences in the data. **C** The UpSet plot presents a segment of the analysis, with the entire content available in Additional file 6. The UpSet plot displays the number of virus clusters that are shared between libraries and those unique to each library. Horizontal bars (purple) represent the number of virus clusters unique to each library. Vertical bars (orange) indicate the number of virus clusters shared between libraries. Dots and lines (gray): identify the specific libraries involved in each intersection. The light green bars in the upper right corner show the proportion of shared and unique virus clusters, respectively. **D** Seasonal differences in total virus diversity (Shannon diversity index). **E** Non-metric multidimensional scaling analysis displays the variations in virus composition between seasons. In the NMDS plots, the circles represent the 95% normal probability ellipse. **F** Virus clusters (biomarkers) contributing to seasonal differences were identified by linear discriminant analysis effect size analysis. LDA score (log) > 2. **G** The heat map shows the relative abundance of virus clusters (biomarkers) in each sample. All virus clusters were classified according to their carriers. The relative abundance of each cluster was calculated as $\log_2(\text{RPM} + 0.5)$. **H** The violin plots show seasonal differences in the relative abundance of insect-related viruses, bird-related viruses, as well as *Coronaviridae* and *Picornaviridae* of mammal-related viruses. The relative abundance of each virus cluster was calculated as $\log_2(\text{RPM} + 1)$

about 16.32% were present in autumn (Fig. 2C). Among the virus clusters shared between samples, about 82.28% were shared within the same season, while about 17.72% were shared between different seasons (Fig. 2C). The

UpSet plot in Fig. 2C presents a segment of the UpSet analysis, with the complete content available in Additional file 16 (Figure S6). However, the bar graph in Fig. 2C was calculated based on 4377 contigs.

No significant seasonal differences in total virus diversity were found within each sampling location ($t = -5.09$ – 6.63 , $P > 0.05$; Fig. 2D). In contrast, we found a significant seasonal variation in beta diversity, which indicated that the total virus composition significantly differed between summer and autumn ($R^2 = 0.07$, $P = 0.002$; Fig. 2E). We excluded the possibility that differences between seasons were influenced by the degree of data dispersion within each season ($P = 0.256$; Additional file 17: Figure S7A). The results of ANOSIM also showed that the differences between seasons were significantly greater than the differences within each season ($R = 0.465$, $P = 0.001$; Additional file 17: Figure S7B). The results also showed that the seasonal variation in virus composition remained significant ($R^2 = 0.07$, $P = 0.004$; Table 1) when sampling location was used as a blocking factor.

The LDA Effect Size (LEfSe) analysis was performed to further identify virus clusters (biomarkers) that were major contributors to the differences between seasons (Fig. 2F). We found that the virus clusters contributing to seasonal differences were mainly insect-, plant-, bird-, and mammal-related viruses (Fig. 2G). The relative abundance of insect-related viruses was significantly higher in summer than in autumn ($t = -4.489$, $P = 7.328e^{-06}$; Fig. 2H). However, the relative abundance of bird-related viruses was significantly higher in autumn than in summer ($t = 7.038$, $P = 2.542e^{-11}$; Fig. 2H). Although the differences in the relative abundance of total mammal-related viruses were not significant between seasons ($t = 1.78$, $P = 0.08$; Additional file 18: Figure S8), the differences in the relative abundance of *Coronaviridae* and *Picornaviridae* in mammal-related viruses were significant. The relative abundance of *Coronaviridae* was significantly greater in summer than in autumn ($t = -4.75$, $P = 4.393e^{-06}$; Fig. 2H), most of which were MERS-related coronavirus (Additional file 12: Table S10). While the relative abundance of *Picornaviridae* was significantly greater in autumn than in summer ($t = 2.78$, $P = 0.006$; Fig. 2H), most of them were *Ia io* picornavirus 1 (Additional file 12: Table S10).

Seasonal variation in dietary diversity and body mass

We obtained 1306 OTUs associated with insects and bird prey after clustering the DNA sequences (Additional file 19: Table S11). These OTUs were annotated to 131 known families belonging to 17 orders (Additional file 19: Table S11). We found significant seasonal differences in prey diversity ($W = 896$, $P = 0.006$; Additional file 20: Figure S9A) and composition ($R^2 = 0.0249$, $P = 0.001$; Additional file 20: Figure S9B). In addition, a higher relative abundance of insect prey was found in summer and bird prey was predominantly present in autumn (Additional file 20: Figure S9C). We also investigated the seasonal differences in body mass and found that there were significant seasonal differences in body mass ($W = 3395$, $P = 2.338e^{-9}$; Additional file 20: Figure S9D).

The relationships between virus diversity and prey diversity

The optimal linear model revealed a significant positive correlation between prey diversity and total virus diversity, explaining 26.5% of the variation in total virus diversity ($R^2_{\text{adjusted}} = 0.265$, $P = 0.017$; Table 2; Fig. 4A). The result of the Mantel test suggested that the similarity in prey composition was significantly positively correlated with the similarity in total virus composition ($R = 0.42$, $P = 1e^{-04}$; Fig. 5A).

We found that the average number of potential new viruses per library was approximately 59 in summer and approximately 14 in autumn (Additional file 21: Table S12). The optimal linear model explained 26.1% of the variation in the number of potential new viruses ($R^2_{\text{adjusted}} = 0.261$; Table 2). The results did not reveal a significant positive correlation between prey diversity and the number of potential new viruses ($P = 0.06$; Table 2; Fig. 4B). However, a negative correlation was observed between body mass and the number of potential new viruses ($P = 0.03$; Table 2; Fig. 4B). The result of the Mantel test suggested that the similarity in prey composition was significantly positively correlated with the number of potential new viruses ($R = 0.39$, $P = 0.002$; Fig. 5B).

(See figure on next page.)

Fig. 3 The co-occurrence patterns and phylogenetic relationships of prey-related virus species. The virus-sharing network reveals co-occurrence patterns of prey-related virus species from 22 known families. In this network, each node represents a season or a virus species. An edge linking a season node and a virus node indicates the presence of that virus in that season. The nodes positioned within the central area of the network plot, encompassed by gray shading, represent virus species that are shared between seasons. The remaining nodes in the network plot indicate virus species that are unique to each season. Phylogenetic trees were estimated using a maximum likelihood method based on a partial amino acid sequence of the RdRp protein

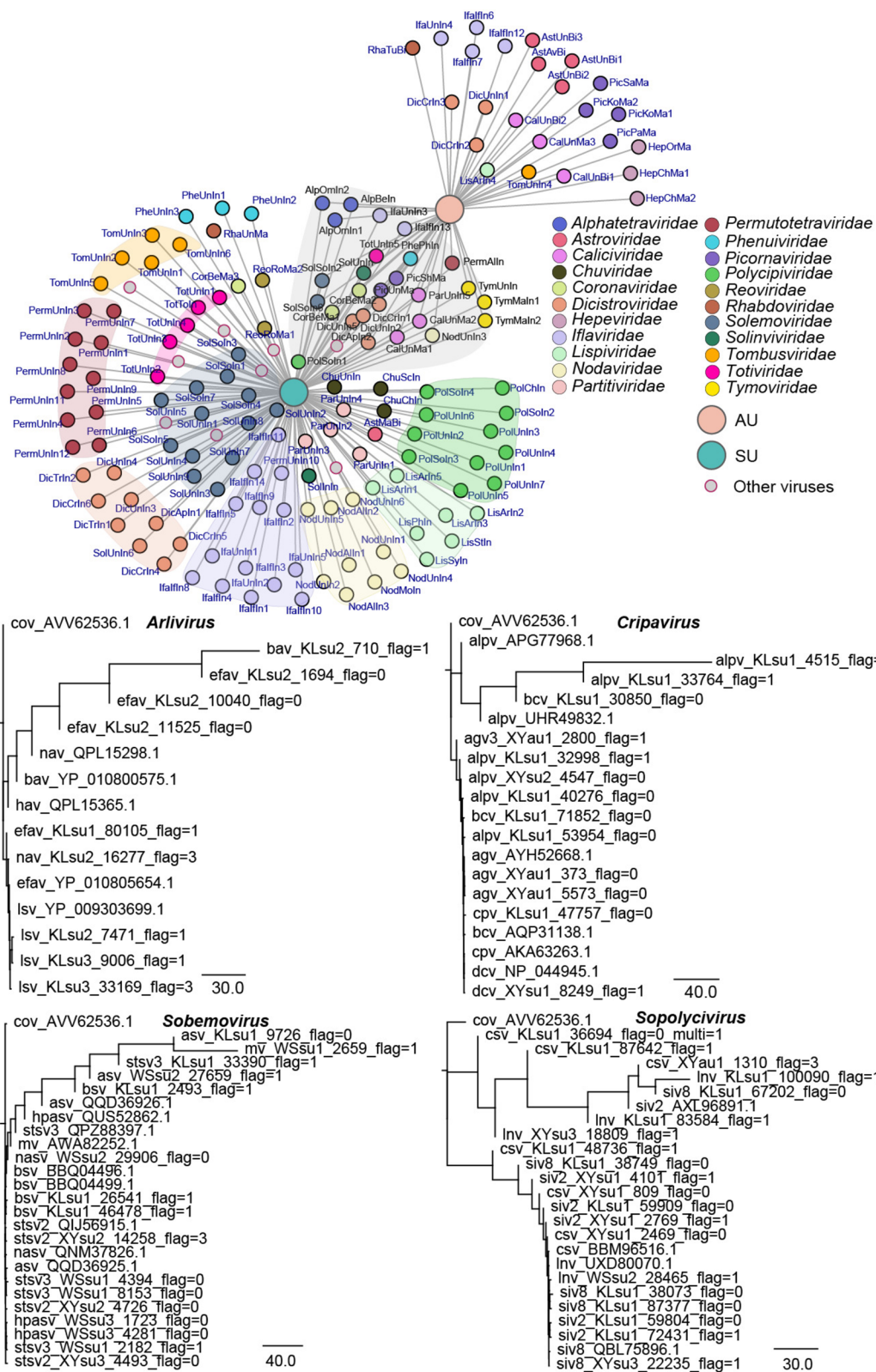


Fig. 3 (See legend on previous page.)

Table 1 The results of permutational multivariate analysis of variance

| | Df | Sum of Sq | R ² | F | Pr (> F) | |
|-----------------|----|-----------|----------------|------|--------------|----|
| Season | 1 | 0.58 | 0.07 | 1.23 | 0.004 | ** |
| Sample location | 2 | 1.09 | 0.13 | 1.14 | 0.004 | ** |
| Residual | 14 | 6.71 | 0.79 | | | |
| Total | 17 | 8.39 | 1.00 | | | |

The bold font in the table is used to highlight significant P-values

Significant: 0****0.001***0.01**0.05*0.1

Table 2 Summary of the optimal linear models

| Model 1: Total virus diversity model; AICc = 48.73 | | | | | |
|--|-------------|------------|---------|----------------|-----|
| Predictors | Estimate | Std. error | z value | Pr(> z) | |
| (Intercept) | 1.86 | 0.47 | 3.97 | 0.001 | ** |
| Prey diversity | 1.34 | 0.50 | 2.67 | 0.017 | * |
| Observations | 18 | | | | |
| R ² /R ² _{adjusted} | 0.308/0.265 | | | | |
| Model 2: Number of potential new virus model; AICc = 13.73 | | | | | |
| Predictors | Estimate | Std. error | z value | Pr(> z) | |
| (Intercept) | 2.27 | 0.85 | 2.56 | 0.01 | * |
| Body mass | -0.02 | 0.01 | 2.06 | 0.03 | * |
| Prey diversity | 0.38 | 0.19 | 1.84 | 0.06 | |
| Observations | 18 | | | | |
| R ² /R ² _{adjusted} | 0.326/0.261 | | | | |
| Model 3: Relative abundance of prey-related virus model; AICc = 21.45 | | | | | |
| Predictors | Estimate | Std. error | z value | Pr(> z) | |
| (Intercept) | 2.72 | 0.63 | 4.03 | < 0.001 | *** |
| Bird prey | -0.09 | 0.05 | 1.66 | 0.09 | |
| Insect prey | 0.51 | 0.12 | 3.93 | < 0.001 | *** |
| Observations | 18 | | | | |
| R ² /R ² _{adjusted} | 0.647/0.613 | | | | |
| Model 4: Relative abundance of <i>Picornaviridae</i> model; AICc = 63.66 | | | | | |
| Predictors | Estimate | Std. error | z value | Pr(> z) | |
| (Intercept) | -1.63 | 1.24 | -1.32 | 0.206 | |
| Prey diversity | 3.55 | 1.07 | 3.33 | 0.005 | ** |
| Bird prey | 0.61 | 0.16 | 3.81 | 0.002 | ** |
| Observations | 18 | | | | |
| R ² /R ² _{adjusted} | 0.501/0.434 | | | | |

Prey diversity represents the diversity of prey hunted by *I. io*, which mainly includes insects and birds. Prey diversity was calculated as the Shannon index of each sample. Body mass represents the average weight of all *I. io* individuals included in each sample. Insect prey represents the relative abundance of insect prey in each sample. Bird prey represents the relative abundance of bird prey in each sample. The bold font in the table is used to highlight significant P-values

Significant: 0****0.001***0.01**0.05*0.1

The relationships between dietary diversity and virus abundance

The optimal linear model for prey-related viruses showed that the relative abundance of insects was significantly positively correlated with the relative abundance of prey-related viruses, explaining 61.3% of the variation

in the relative abundance of prey-related viruses ($R^2_{\text{adjusted}} = 0.613$, $P < 0.001$; Table 2; Fig. 4C). The results of linear regression showed that prey abundance was positively correlated with the relative abundance of prey-related viruses in summer and autumn (summer: $R^2 = 0.4$, $P = 0.04$; autumn: $R^2 = 0.63$, $P = 0.0002$; Fig. 5C). There was no significant correlation between the relative abundances of *Coronaviridae* and *Ia io* picornavirus 1 and body mass, prey diversity, and the relative abundances of insect and bird prey ($P > 0.05$; Additional file 22: Table S13). However, the optimal linear model of *Picornaviridae* revealed that prey diversity and the relative abundance of bird prey were significantly positively correlated with the relative abundance of *Picornaviridae*, and explained 43.4% of the variation in total ($R^2_{\text{adjusted}} = 0.434$; prey diversity: $P = 0.005$, bird prey: $P = 0.002$; Table 2; Fig. 4D).

Discussion

In this study, we performed DNA metabarcoding sequencing and viral metatranscriptomic sequencing to characterize the seasonal variations in dietary diversity and RNA virus diversity of three *I. io* populations in Southwest China and assess the relationships between dietary diversity and RNA virus diversity. First, seasonal differences in dietary diversity and RNA virus diversity in *I. io* were detected, with a relatively high relative abundance of insect prey and insect-related viruses in summer and various bird prey and bird-related viruses predominantly present in autumn, supporting our first prediction of the first hypothesis. Second, a significant positive correlation was identified between prey diversity and total viral diversity. The more similar the prey composition, the more similar the total viral composition and the greater the number of potential novel viruses, supporting our second prediction of the first hypothesis. Finally, the significant positive correlation between the relative abundance of insect prey and prey-related viruses of *I. io*, as well as between prey diversity and the relative abundance of bird prey and *Picornaviridae*, supported our final prediction of the first hypothesis. Moreover, no connection between body mass and total virus diversity was observed, but a significant negative correlation with

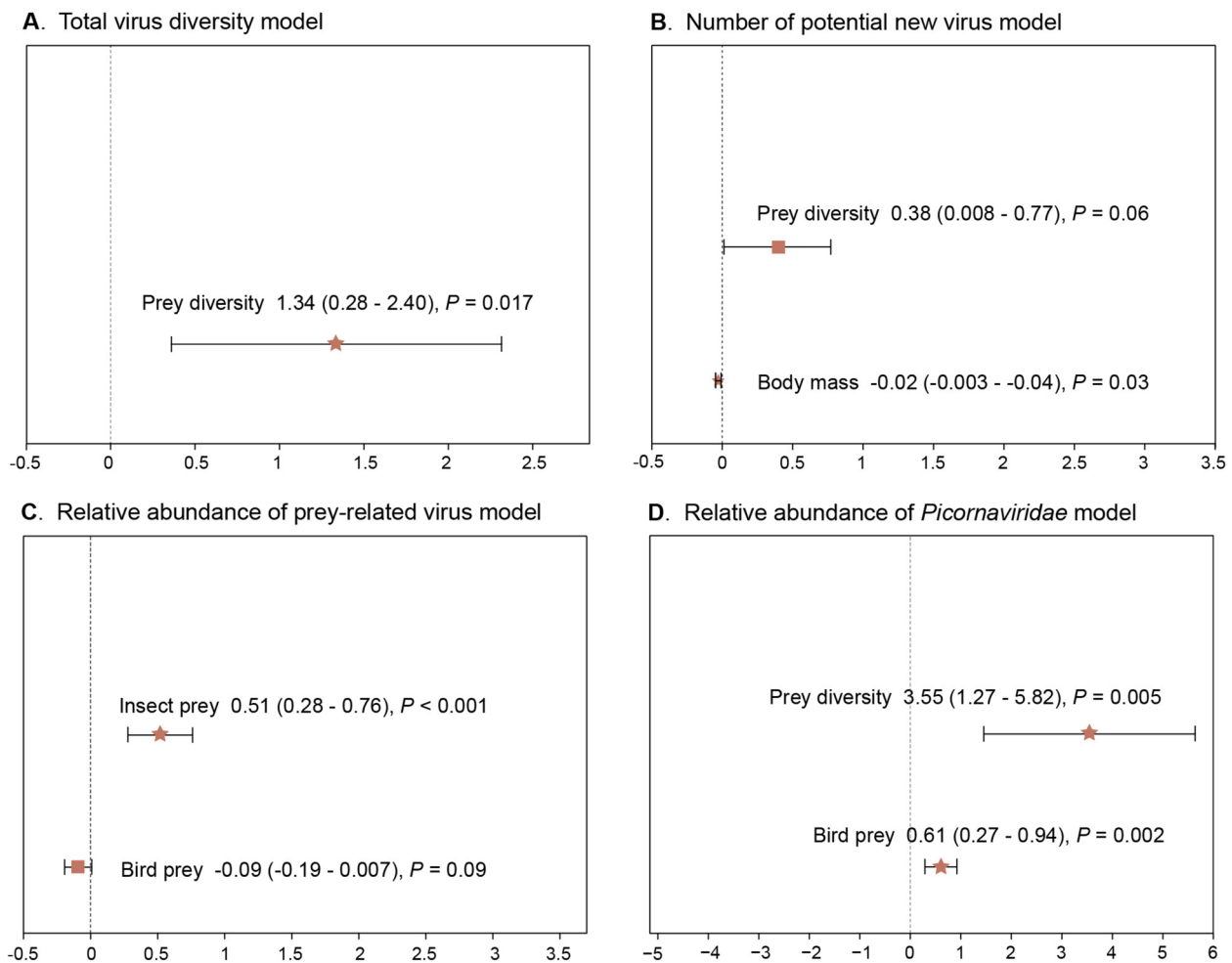


Fig. 4 The forest plot for the optimal models. The regression coefficient is shown for each factor with 95% confidence intervals. Factors that remained significant in the optimal model are shown as a pentagram. Models were constructed for **A** the total virus diversity, **B** the number of potential new viruses, **C** the relative abundance of prey-related viruses, and **D** the relative abundance of *Picornaviridae*

the number of potential new viruses was noted, providing partial support for our prediction of the second hypothesis.

Some studies found that insectivorous bats carry highly diverse RNA virus species, with a large number of insect-related viruses, besides those associated with mammals [11, 78–80], such as *Polyciviridae*, *Permutotetraviridae*, *Baculoviridae*, *Iflaviridae*, *Dicistroviridae*, and *Tetraviridae*. Similarly, we found that *I. io* carried various RNA viruses belonging to 55 genera and 35 known virus families. Among them, the relative abundance of virus families associated with insects was particularly prominent, such as *Polyciviridae*, *Dicistroviridae*, *Permutotetraviridae*, *Iflaviridae*, and *Alphatetraviridae*. Most carriers of these viruses that we detected were from various insect orders, such as Lepidoptera, Diptera, Hymenoptera, and Hemiptera. We subsequently found that the relative abundance of insect-related viruses was higher in

summer than in autumn. In contrast, we detected various bird-related viruses in bats during autumn, when they prey on birds, and the relative abundance of bird-related viruses was higher in autumn than in summer. We also confirmed that the carriers of these viruses included various families in Passeriformes, such as Sylviidae, Emberizidae, Muscicapidae, Fringillidae, and Zosteropidae. This might be related to the changes in the dietary structure of *I. io*, which mainly feeds on insects in summer and passerine birds in autumn. Overall, these results implied a significant link between the seasonal differences in the virus diversity and dietary diversity of *I. io* (insects in summer and mainly birds in autumn), possibly because *I. io* mainly prey on insects in summer and birds in autumn. Moreover, some viruses in *I. io* may persist across seasons because approximately 20% of the viral species are shared between populations across seasons. Thus, we showed that viruses may spread among organisms via dynamic

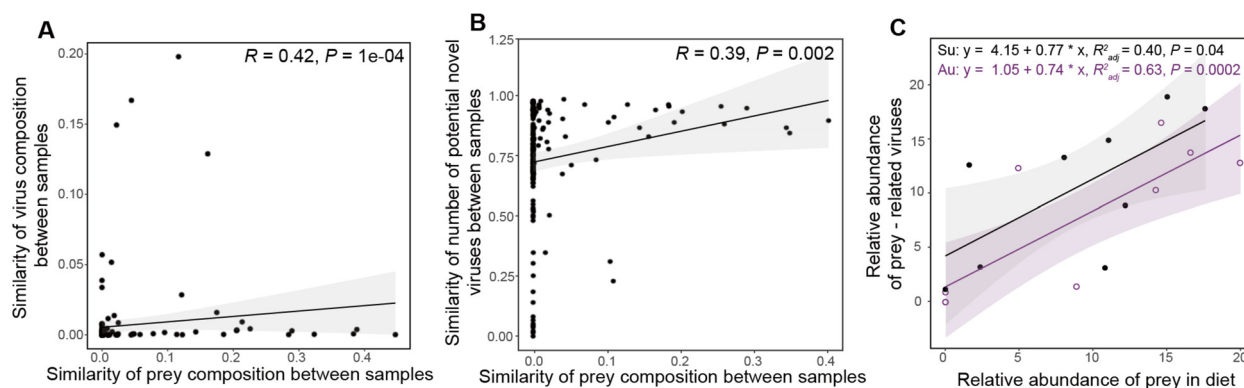


Fig. 5 Effect of dietary diversity on virus diversity. **A** The Mantel test shows the relationship between prey species composition and virus species composition of *I. io*. Each black dot represents the similarity between the two samples. The similarity was calculated as “1-Bray_Curtis_distance”. **B** The Mantel test shows the relationship between prey species composition and the number of potential new viruses. Each black dot represents the similarity between the libraries. The similarities in the prey species composition were calculated as “1-Bray_Curtis_distance”. The similarities in the number of potential new viruses were calculated as “1-euclidean_distance/max(euclidean_distance)”. **C** The relationship between the relative abundance of prey and the relative abundance of prey-related viruses. Different colors represent different seasons; black indicates summer, and purple indicates autumn

changes in predator–prey interactions within a season and among seasons. However, future studies are needed to find direct evidence of a biological interaction between these viruses and the predators.

Virus richness and abundance may be driven by host traits, including body mass, age, sex, behavior, host order, etc. [10–13, 19]. In this study, no significant association was found between total virus diversity and body mass of *I. io*. This finding appears to deviate from previous results at the species level, as prior studies have shown positive correlations between body mass and virus richness [12, 81, 82]. This can be attributed to larger species having a greater surface area, wider geographical scope, and longer lifespan, which enables them to come into contact with and accumulate more viruses [12, 19]. In this case, changes in body mass may not have a substantial effect on the seasonal variation of total virus diversity in *I. io* at the population level. Instead, other ecological factors are more likely. The results of this study revealed a significant negative correlation between body mass and the number of potential new viruses. We formulated two hypotheses regarding the potential factors that might have influenced this outcome. The first factor is that a lower body mass indicates compromised immunity, thereby increasing susceptibility or adaptability to viruses and ultimately fostering the emergence of potential new viruses. However, we are inclined to the fact that bats with smaller body mass are concentrated in the summer, which is affected by greater total virus diversity and, therefore, increases the number of potential new viruses. Of course, confirmation of this relationship requires further research to gain a more comprehensive understanding of the impact of body mass on virus diversity.

The diversity of viruses shows phylogenetic, temporal, and spatial heterogeneity because of the influence of the ecological factors of carriers [10, 11, 13, 83]. For example, predator–prey interactions and diet may influence the virome composition, especially at higher taxonomic levels [10]. The virus diversity of *Desmodus rotundus* shows an elevational gradient and decreases with local anthropogenic food resources, as measured by livestock density [13]. Here we also found that high prey diversity significantly increased total virus diversity. Additionally, similar dietary compositions indicated similar virus compositions. This finding was attributed mainly to the fact that interactions mediated by predation between the predator and other animals occur widely and frequently throughout the lifespan of predators [28, 84–89]. We speculated that predation on diverse prey exposes predators to a greater number and variety of prey-related viruses. In this study, we provided evidence for this speculation by finding that the relative abundance of prey-related viruses increased significantly with increasing insect prey abundance. Additionally, consuming a greater variety and complexity of prey species may increase the chances of interactions among various viruses, and thus may further facilitate virus evolution [28, 90, 91], particularly for closely related virus species [92]. We also found that the more similar the prey composition, the greater the similarity of the number of potential new viruses in *I. io*. These results further imply the hypothesis of an association between predator-mediated virus aggregation and virus diversity. Certainly, this needs to be focused and confirmed on in future studies.

The resource allocation hypothesis states that investing more resources into one activity may result in a decrease in resource allocation in other areas [93, 94]. We found

a significant positive correlation between prey diversity and the relative abundance of *Picornaviridae*. Higher prey diversity may indirectly indicate that individuals of *I. io* spend more time and energy searching for prey. This occurs probably because different prey species may be distributed in different regions and habitats, or they may have different behavioral habits that require different hunting strategies by predators. In this case, predators that spend more time searching for prey may allocate fewer resources to the immune system [93]. This may increase their susceptibility to viruses, and thus, an increase in their relative abundance. However, further studies are needed to elucidate the mechanisms underlying the effects of prey diversity on the relative abundance of different viruses.

Whether the presence of numerous insect-related and bird-related viruses in *I. io* increases their infection rates needs to be determined in the future. Two studies reported that the spread of viruses via predator–prey interactions among distantly related species is transient, implying that these viruses may exist in the digestive system of predators for a short period of time [10, 33]. These viruses cannot lead to infections in predators. However, several studies have provided an alternative view. For example, western red colobus monkeys (*P. badiussimian*) can transfer foamy viruses (SFV) to wild chimpanzees (*P. verus*) because the monkeys are regularly hunted by the chimpanzees. Two new influenza A viruses (H17N10 and H18N11) were found in bats [95, 96]. However, the main natural reservoir of influenza viruses is thought to be birds. The detection of influenza virus in bats suggests that any association between bats and birds (e.g., predation, living in the same habitat) may facilitate the transmission of influenza viruses. Additionally, a large number of viruses previously thought to be invertebrate-specific or invertebrate-associated, which exhibit multiorgan distributions within the organs of shrews, bats, and rodents, have been identified [11]. These findings suggest that these viruses are likely to replicate efficiently within the wildlife. Various arthropods are known to constitute a part of the diet of these wild animals, particularly shrews and bats. Thus, although most prey-related viruses are typically considered to not infect these predators owing to their host specificity and distant relatives, the possibility of cross-infection cannot be rejected if prey-related viruses achieve efficient evolution or recombination in predators [33, 91, 97]. Most arguments supporting predation as a presumed transmission route are based on observations, experimental studies, and/or phylogenetic analysis of top predators [89, 98–101]. Future studies should conduct viral metagenomic analysis of the entire food web and test viral biological activity in wild animals to determine the patterns of the virus transmission networks in communities and ecosystems [33].

Conclusions

To summarize, this investigation explored the variation in the RNA virus diversity of *I. io* across different seasons and assessed the links between dietary diversity and RNA virus diversity. We found seasonal differences both in dietary diversity and RNA virus diversity in *I. io*, with a relatively high relative abundance of insect prey and insect-related viruses in summer and various bird prey and bird-related viruses predominantly present in autumn. Our results also revealed a significant correlation between RNA virus diversity and dietary diversity of *I. io*. We found that the relative abundance of *Picornaviridae* increased with increasing prey diversity and body mass. These results confirmed the evident relationships between virus diversity and prey diversity in bats and highlighted the potential roles of predator–prey interactions in shaping virus diversity. However, this study had a major limitation. The direct separation of prey-related viruses from the organs of *I. io* was not achieved, although noninvasive viral metatranscriptomic sequencing indicated a high abundance of prey-related viruses. Consequently, direct evidence supporting effective biological interaction between prey-related viruses and *I. io* was lacking. Therefore, additional experiments should be conducted in future studies to investigate the potential biological processes underlying the association between prey diversity and virus diversity and to determine the infection rate associated with virus transmission from prey to predator. This could include negative strand detection for positive-strand RNA viruses, laboratory experiments, and virus isolation.

Abbreviations

| | |
|--------------|--|
| COVID-19 | Coronavirus disease 2019 |
| EID | Emerging infectious diseases |
| SFV | Simian foamy viruses |
| ASAB | Association for the study of animal behavior |
| ABS | Animal Behavior Society |
| XY | Xingyi City, Guizhou Province |
| KL | Kaili City, Guizhou Province |
| WS | Weishan County, Yunnan Province |
| XYsu1 | The first library of Xingyi City in the summer |
| RefSeq-based | Reference sequence-based |
| EVRD | The eukaryotic viral reference database |
| RdRp | RNA-dependent RNA polymerase |
| ML | Maximum likelihood |
| RPM | The number of viruses reads per million from the total reads in each library |
| COI | Cytochrome oxidase I |
| OTUs | Operational taxonomic units |
| NMDS | Non-metric Multidimensional Scaling |
| ANOSIM | Analysis of similarities |
| LEfSe | Linear discriminant analysis effect size |
| LDA | Linear discriminant analysis |
| LM | Linear regression model |
| VIF | Variance inflation factor |
| SARS-related | Severe acute respiratory syndrome-related |

Supplementary Information

The online version contains supplementary material available at <https://doi.org/10.1186/s40168-024-01950-6>.

Additional file 1: Table S1. Sequences of primers and the result in RT-PCR (Reverse Transcription PCR) experiment.

Additional file 2: Figure S1. Validation of viral metagenomic sequencing results by nested reverse transcription PCR (RT-PCR). (A) The relationship between the relative abundance and the positive rate of 11 virus species. The positive rate for each virus was calculated as the “number of positive samples in each library/total number of each library. alpV: aphid lethal paralysis virus; wcv1: wuhan coneheads virus 1; gnv2: guiyang nodavirus 2; ps1: picornaviridae sp. 1; ps2: picornaviridae sp. 2; bmiv: bombyx mori iflavivirus; aa: avian astrovirus; aspv4: avian associated picorna-like virus 4; pav1: passerine astrovirus 1; pav3: passerine astrovirus 3; pav4: passerine astrovirus 4. (B) Gel electrophoresis results of nested RT-PCR. The green squares represent positive samples. The words above the gel electrophoresis diagram mean “the name of viruses - the library name - the ID of the positive sample”.

Additional file 3: Table S2. The candidate models of LM and LMM for the total virus diversity.

Additional file 4: Table S3. The candidate models of LM and LMM for the number of potential new virus.

Additional file 5: Table S4. The candidate models of LM and LMM for the relative abundance of prey-related virus.

Additional file 6: Table S5. The candidate models of LM and LMM for the relative abundance of *Picornaviridae*.

Additional file 7: Table S6. The candidate models of LM and LMM for the relative abundance of *Coronaviridae*.

Additional file 8: Table S7. The candidate models of LM and LMM for the relative abundance of *Ia io* picornavirus 1.

Additional file 9: Table S8. Summary of the optimal linear mixed models.

Additional file 10: Table S9. The information of bats used in this study and the establishment of libraries in viral metagenomic analysis.

Additional file 11: Figure S2. The amount of raw sequencing data for each library.

Additional file 12: Table S10. Taxonomic information and the relative abundance of viruses identified in *Ia io*.

Additional file 13: Figure S3. Phylogenetic analysis of bird-related viruses belonging to the family *Caliciviridae*. The phylogenetic tree was constructed based on the amino acid sequences of the RdRp protein of *Caliciviridae* found in this study. The bird-related virus contigs found in this study were marked with magenta circles. The virus sequences were aligned using MAFFT version 7.48. The phylogenetic trees were constructed in IQ-TREE version 2.0 based on the maximum likelihood (ML) approach. The best-fit amino acid substitution model for the phylogenetic tree was WAG+F+I+G4, as determined by BIC.

Additional file 14: Figure S4. Phylogenetic analysis of bird-related viruses belonging to the family *Astroviridae*. The phylogenetic tree was constructed based on the amino acid sequences of the RdRp protein of *Astroviridae* determined in this study. Within trees, the bird-related virus contigs found in this study were marked with orange circles. The virus sequences were aligned using MAFFT version 7.48. The phylogenetic trees were constructed using IQ-TREE version 2.0 based on the maximum likelihood (ML) approach. The best-fit amino acid substitution model for the phylogenetic tree was VT+F+I+G4, as determined by BIC.

Additional file 15: Figure S5. A phylogenetic analysis of *Picornaviridae* was performed in this study. The phylogenetic tree was constructed based on the amino acid sequences of the RdRp protein of *Picornaviridae* determined in this study. Within trees, the bird-related virus contigs found in this study were marked with green circles. The virus sequences were aligned using MAFFT version 7.48. The phylogenetic trees were constructed using IQ-TREE version 2.0 based on the maximum likelihood (ML)

approach. The best-fit amino acid substitution model for the phylogenetic tree was JTTDCMut+F+I+G4, as determined by BIC.

Additional file 16: Figure S6. The UpSet plot displays the number of virus clusters that are shared between libraries and those unique to each library. Horizontal Bars: Represent the number of virus clusters unique to each library. Vertical Bars: Indicate the number of virus clusters shared between libraries. Dots and Lines: Identify the specific libraries involved in each intersection.

Additional file 17: Figure S7. The exclusion of the influence of differences among samples within season on inter-seasonal differences. (A) PERMANOVA was performed to study the significance of the dispersion of samples within each season. (B) Analysis of similarities (ANOSIM) was performed to evaluate the magnitude of differences in virus species composition between and within seasons. *R* value indicated the ANOSIM statistic. The *R* values ranged from -1 to 1, and were interpreted along with the *P* values in this analysis. *R* closed to 1 and *P*.

Additional file 18: Figure S8. Seasonal variation in the relative abundance of total mammal-related viruses. The relative abundance of each virus cluster was calculated as \log_2 (RPM+1).

Additional file 19: Table S11. Taxonomic information and abundance of prey identified in *Ia io*.

Additional file 20: Figure S9. Seasonal variation in dietary diversity and body mass. AU indicates autumn (shown in pink); SU indicates summer (shown in blue). Each dot represents the data for an individual bat. (A) Seasonal differences in prey diversity were represented by the Shannon diversity index. Each solid black circle represents the Shannon diversity index for each bat. (B) Non-Metric Multidimensional Scaling analysis of the variation in species composition in the diet between seasons. In the NMDS plots, circles represent the 95% normal probability ellipse for each season. (C) The horizontal histogram shows the relative abundance of prey as a proportion of each bat individual. Different colors represent different seasons. (D) Seasonal differences in body mass of bats.

Additional file 21: Table S12. Result of blastx for hallmark genes of potential new virus species (Amino acid identity < 90%). Table S12. Summary of the optimal linear mixed models.

Additional file 22: Table S13. Summary of the optimal linear models.

Acknowledgements

We thank Xiaomin Yan for assisting in the laboratory work, Yuhang Liu and Yang Liu for preprocessing and annotation of raw data from viral metagenomic sequencing.

Authors' contributions

Original idea of the study by ZLY H and TL J; ZLY H, ZQ W, YY L and CK carried out field experiments. ZLY H analyzed the data and wrote the manuscript. TL J and JF revised the manuscript. BH had an effective discussion on the manuscript. All authors contributed to the writing of the paper and gave final approval for publication.

Funding

This research was supported by the Fundamental Research Funds for the Central Universities (2412023YQ002), the National Natural Science Foundation of China (Grant Nos. 32371562, 32192424), the Key consulting research project of Jilin Research Institute of Chinese Academy of Engineering (JL2023-02), the Fund of the Jilin Province Science and Technology Development Project (Grant No. 20220101273JC), and the Special Foundation for National Science and Technology Basic Research Program of China (2021FY100301).

Data availability

RNA sequencing raw data were deposited into CNGB Sequence Archive (CNSA) of China National GeneBank database (CNGBdb) under accession number CNP0005310. RNA sequencing raw data can also obtain from the SRA database of National Center for Biotechnology Information (NCBI) under BioProject accession number PRJNA1081129.

Declarations

Ethics approval and consent to participate

This study adhered to the ASAB/ABS Guidelines for the Use of Animals in Research. All experimental procedures in this study were approved by the Science and Technology Ethics Committee of Northeast Normal University, China (approval number NENU-2019-04).

Consent for publication

Not applicable.

Competing interests

The authors declare no competing interests.

Author details

¹Jilin Provincial Key Laboratory of Animal Resource Conservation and Utilization, Northeast Normal University, 2555 Jingyue Street, Changchun 130117, China. ²Key Laboratory of Vegetation Ecology of Education Ministry, Institute of Grassland Science, Northeast Normal University, 5268 Renmin Avenue, Changchun 130024, China. ³College of Life Science, Jilin Agricultural University, 2888 Xincheng Street, Changchun 130118, China. ⁴Changchun Veterinary Research Institute, Chinese Academy of Agricultural Sciences, Changchun, Jilin Province, China.

Received: 26 February 2024 Accepted: 14 October 2024

Published online: 23 November 2024

References

- Sun J, He WT, Wang L, Lai A, Ji X, Zhai X, et al. COVID-19: epidemiology, evolution, and cross-disciplinary perspectives. *Trends Mol Med*. 2020;26(5):483–95.
- Zheng Z, Lu Y, Short KR, Lu J. One health insights to prevent the next HxNy viral outbreak: learning from the epidemiology of H7N9. *BMC Infect Dis*. 2019;19(1):138.
- Zumla A, Hui DS, Perlman S. Middle East respiratory syndrome. *The Lancet*. 2015;386(9997):995–1007.
- Zhong NS, Zheng BJ, Li YM, Poon, Xie ZH, Chan KH, et al. Epidemiology and cause of severe acute respiratory syndrome (SARS) in Guangdong, People's Republic of China February 2003. *Lancet*. 2003;362(9393):1353–8.
- Tian J, Sun J, Li D, Wang N, Wang L, Zhang C, et al. Emerging viruses: Cross-species transmission of coronaviruses, filoviruses, henipaviruses, and rotaviruses from bats. *Cell Rep*. 2022;39(11).
- Jones KE, Patel NG, Levy MA, Storeygard A, Balk D, Gittleman JL, et al. Global trends in emerging infectious diseases. *Nature*. 2008;451(7181):990–3.
- Wu Z, Yang L, Ren X, He G, Zhang J, Yang J, et al. Deciphering the bat virome catalog to better understand the ecological diversity of bat viruses and the bat origin of emerging infectious diseases. *ISME J*. 2016;10(3):609–20.
- Shi M, Lin XD, Chen X, Tian JH, Chen LJ, Li K, et al. The evolutionary history of vertebrate RNA viruses. *Nature*. 2018;556(7700):197–202.
- Shi M, Lin XD, Tian JH, Chen LJ, Chen X, Li CX, et al. Redefining the invertebrate RNA virosphere. *Nature*. 2016;540(7634):539–43.
- French RK, Anderson SH, Cain KE, Greene TC, Minor M, Miskelly CM, et al. Host phylogeny shapes viral transmission networks in an island ecosystem. *Nat Ecol Evol*. 2023;7(11):1834–43.
- Chen YM, Hu SJ, Lin XD, Tian JH, Lv JX, Wang MR, et al. Host traits shape virome composition and virus transmission in wild small mammals. *Cell*. 2023;186(21):4662–75.
- Yin S, Li N, Xu W, Becker DJ, de Boer WF, Xu C, et al. Functional traits explain waterbirds' host status, subtype richness, and community-level infection risk for avian influenza. *Ecol Lett*. 2023;26(10):1780–91.
- Bergner LM, Orton RJ, Benavides JA, Becker DJ, Tello C, Biek R, et al. Demographic and environmental drivers of metagenomic viral diversity in vampire bats. *Mol Ecol*. 2020;29(1):26–39.
- Ni XB, Pei Y, Ye YT, Shum MHH, Cui XM, Wu YQ, et al. Ecoclimate drivers shape virome diversity in a globally invasive tick species. *ISME J*. 2024;18(1):wrae087.
- Liu Q, Cui F, Liu X, Fu Y, Fang W, Kang X, et al. Association of virome dynamics with mosquito species and environmental factors. *Microbiome*. 2023;11(1):101.
- Wang J, Pan YF, Yang LF, Yang WH, Lv K, Luo CM, et al. Individual bat virome analysis reveals co-infection and spillover among bats and virus zoonotic potential. *Nat Commun*. 2023;14(1):4079.
- Lindstedt SL, Miller BJ, Buskirk SWJE. Home range, time, and body size in mammals. *Ecology*. 1986;67(2):413–8.
- Palomares FJCoZ. Site fidelity and effects of body mass on home-range size of Egyptian mongooses. *Can J Zool*. 1994;72(3):465–9.
- Smith OM, Snyder WE, Owen JPBR. Are we overestimating risk of enteric pathogen spillover from wild birds to humans? *Biol Rev*. 2020;95(3):652–79.
- Speakman JRJoEB. Body size, energy metabolism and lifespan. *J Exp Biol*. 2005;208(9):1717–30.
- Warmuth VM, Metzler D, Zamora-Gutierrez V. Human disturbance increases coronavirus prevalence in bats. *Sci Adv*. 2023;9(13):eadd0688.
- Caron A, Garine-Wichatitsky MD, Gaidet N, Chivweshe N, Cumming GS. Estimating dynamic risk factors for pathogen transmission using community-level bird census data at the wildlife/domestic interface. *Ecol Soc*. 2010;15(3):25.
- Raghwani J, Faust CL, François S, Nguyen D, Marsh K, Raulo A, et al. Seasonal dynamics of the wild rodent faecal virome. *Mol Ecol*. 2022;32(17):4763–76.
- Turmelle AS, Olival KJE. Correlates of viral richness in bats (order Chiroptera). *EcoHealth*. 2009;6:522–39.
- Guy C, Thiagavel J, Mideo N, Ratcliffe JMRSOS. Phylogeny matters: revisiting a comparison of bats and rodents as reservoirs of zoonotic viruses'. *R Soc Open Sci*. 2019;6(2):181182.
- Luis AD, Hayman DT, O'Shea TJ, Cryan PM, Gilbert AT, Pulliam JR, et al. A comparison of bats and rodents as reservoirs of zoonotic viruses: are bats special? *Proc R Soc B: Biol Sci*. 2013;280(1756):20122753.
- Gay N, Olival KJ, Bumrungsri S, Siriaronrat B, Bourgeois M, Morand SJJfPP, et al. Parasite and viral species richness of Southeast Asian bats: Fragmentation of area distribution matters. *Int J Parasitol: Parasites Wildl*. 2014;3(2):161–70.
- Leendertz FH, Zirkel F, Couacy-Hymann E, Ellerbrok H, Morozov VA, Pauli G, et al. Interspecies transmission of simian foamy virus in a natural predator-prey system. *J Virol*. 2008;82(15):7741–4.
- Molsher R, Gifford E, McLlroy JJWR. Temporal, spatial and individual variation in the diet of red foxes (*Vulpes vulpes*) in central New South Wales. *Wildl Res*. 2000;27(6):593–601.
- Araújo M, Bolnick D, Martinelli LA, Giaretta AA, Dos Reis SJJoaE. Individual-level diet variation in four species of Brazilian frogs. 2009;78(4):848–56.
- Gong LX, Gu H, Chang Y, Wang ZQ, Shi B, Lin AQ, et al. Seasonal variation of population and individual dietary niche in the avivorous bat. *la io Oecologia*. 2023;201(3):733–47.
- Gong LX, Shi BY, Wu H, Feng J, Jiang TL. Who's for dinner? Bird prey diversity and choice in the great evening bat. *la io Ecol Evol*. 2021;11(13):8400–9.
- French RK, Holmes EC. An Ecosystems Perspective on Virus Evolution and Emergence. *Trends Microbiol*. 2020;28(3):165–75.
- Jan Z, Wilson D, Mittermeier R. *Handbook of the Mammals of the World-Vol. 9. Bats*. *J Vertebr Biol*. 2020;100:335.
- Chan JF, To KK, Tse H, Jin DY, Yuen KY. Interspecies transmission and emergence of novel viruses: lessons from bats and birds. *Trends Microbiol*. 2013;21(10):544–55.
- Nabi G, Wang Y, Lu L, Jiang C, Ahmad S, Wu Y, et al. Bats and birds as viral reservoirs: a physiological and ecological perspective. *Sci Total Environ*. 2021;754:142372.
- Mollentze N, Streicker DG. Viral zoonotic risk is homogenous among taxonomic orders of mammalian and avian reservoir hosts. *PNAS*. 2020;117(17):9423–30.

38. Gong LX, Geng Y, Wang ZQ, Lin AQ, Wu H, Feng L, et al. Behavioral innovation and genomic novelty are associated with the exploitation of a challenging dietary opportunity by an avivorous bat. *iSci*. 2022;25(9):104973.
39. Heim O, Puisto AI, Fukui D, Vesterinen EJ. Molecular evidence of bird-eating behavior in *Nyctalus aviator*. *Acta Ethol*. 2019;22:223–6.
40. Ibanez C, Popa-Lisseanu AG, Pastor-Bevia D, Garcia-Mudarra JL, Juste J. Concealed by darkness: interactions between predatory bats and nocturnally migrating songbirds illuminated by DNA sequencing. *Mol Ecol*. 2016;25(20):5254–63.
41. Ibáñez C, Fukui D, Popa-Lisseanu A, Pastor-Beviá D, García-Mudarra J, Juste J. Molecular identification of bird species in the diet of the bird-like noctule in Japan. *J Zool*. 2021;313(4):276–82.
42. Fukui D, Dewa H, Katsuta S, Sato A. Bird predation by the birdlike noctule in Japan. *J Mammal*. 2013;94(3):657–61.
43. Wang ZQ, Gong LX, Huang ZLY, Geng Y, Zhang WJ, Si M, et al. Linking changes in individual specialization and population niche of space use across seasons in the great evening bat (*Ia io*). *Mov Ecol*. 2023;11(1):32.
44. Andrews S. *FastQC: a quality control tool for high throughput sequence data*. Cambridge, United Kingdom: Babraham Institute; 2010.
45. Bolger AM, Lohse M, Usadel J. Trimmomatic: a flexible trimmer for Illumina sequence data. *Bioinformatics*. 2014;30(15):2114–20.
46. Langmead B, Salzberg SL. Fast gapped-read alignment with Bowtie 2. *Nat Methods*. 2012;9(4):357–9.
47. Wood DE, Lu J, Langmead B. Improved metagenomic analysis with Kraken 2. *Genome Biol*. 2019;20:1–13.
48. Li D, Liu CM, Luo R, Sadakane K, Lam T-W. MEGAHIT: an ultra-fast single-node solution for large and complex metagenomics assembly via succinct de Bruijn graph. *Bioinformatics*. 2015;31(10):1674–6.
49. Chen JJ, Sun Y, Yan XM, Ren ZL, Wang GS, Liu YH, et al. Elimination of foreign sequences in eukaryotic viral reference genomes improves the accuracy of virome analysis. *Msystems*. 2022;7(6):e00907–e922.
50. Buchfink B, Xie C, Huson DH. Fast and sensitive protein alignment using DIAMOND. *Nat Methods*. 2015;12(1):59–60.
51. Chen JJ, Yan XM, Sun Y, Ren ZL, Yan GZ, Wang GS, et al. De-heterogeneity of the eukaryotic viral reference database (EVRD) improves the accuracy and efficiency of viromic analysis. *BioRxiv*. 2022;03:482774.
52. He B, Gong WJ, Yan XM, Zhao ZH, Yang LE, Tan Z, et al. Viral metagenome-based precision surveillance of pig population at large scale reveals viromic signatures of sample types and influence of farming management on pig virome. *Msystems*. 2021;6(3):e00420–e421.
53. Sun Y, Qu YG, Yan XM, Yan GZ, Chen JJ, Wang GS, et al. Comprehensive evaluation of RNA and DNA viromic methods based on species richness and abundance analyses using marmot rectal samples. *Msystems*. 2022;7(4):e00430–e522.
54. *Taxonomy IV. The ICTV Report on Virus Classification and Taxon Nomenclature*. 2019.
55. Schoch CL, Ciufo S, Domrachev M, Hotton CL, Kannan S, Khovanskaya R, et al. NCBI Taxonomy: a comprehensive update on curation, resources and tools. *Database*. 2020;2020:baaa062.
56. <https://www.ncbi.nlm.nih.gov/GenBank>. Accessed May 2023.
57. Katoh K, Standley DM. MAFFT multiple sequence alignment software version 7: improvements in performance and usability. *Mol Biol Evol*. 2013;30(4):772–80.
58. Nguyen L-T, Schmidt HA, Von Haeseler A, Minh BQ. IQ-TREE: a fast and effective stochastic algorithm for estimating maximum-likelihood phylogenies. *Mol Biol Evol*. 2015;32(1):268–74.
59. Rambaut A, FigTree [<https://www.tree.bio.ed.ac.uk/software/figtree/>]. 2017, Accessed.
60. Ling ST, Xing YS, Ning WH, Hao W, Ju Z, Ga G, et al. Virome in the cloaca of wild and breeding birds revealed a diversity of significant viruses. *Microbiome*. 2022;10(1):60.
61. Kolde R, Raivo KM. Package 'pheatmap'. R package. 2015;1(7):790.
62. Wickham H. *ggplot2*. Wiley interdisciplinary reviews: computational statistics. 2011;3(2):180–185.
63. Alberdi A, Aizpurua O, Gilbert MTP, Bohmann K. Scrutinizing key steps for reliable metabarcoding of environmental samples. *Methods Ecol Evol*. 2018;9(1):134–47.
64. Chang Y, Song SJ, Li AQ, Zhang Y, Li ZL, Xiao YH, et al. The roles of morphological traits, resource variation and resource partitioning associated with the dietary niche expansion in the fish-eating bat *Myotis pilosus*. *Mol Ecol*. 2019;28(11):2944–54.
65. Vrijenhoek R. DNA primers for amplification of mitochondrial cytochrome c oxidase subunit I from diverse metazoan invertebrates. *Mol Mar Biol Biotechnol*. 1994;3(5):294–9.
66. Zeale MR, Butlin RK, Barker GL, Lees DC, Jones G. Taxon-specific PCR for DNA barcoding arthropod prey in bat faeces. *Mol Ecol Resour*. 2011;11(2):236–44.
67. Liu YY, Si M, Huang ZLY, Feng J, Jiang TL. Bats are sentinels for invasive pest surveillance based on DNA metabarcoding. *Ecol Ind*. 2023;152:110354.
68. Magoč T, Salzberg SL. FLASH: fast length adjustment of short reads to improve genome assemblies. *Bioinformatics*. 2011;27(21):2957–63. <https://www.boldsystems.org/>. Accessed May 2023.
69. Oksanen J, Kindt R, Legendre P, O'Hara B, Stevens MHH, Oksanen MJ, et al. The vegan package. *Community Ecol Package*. 2007;10(631–637):719.
70. Dag O, Dolgun A, Konar NM. Onewaytests: An R Package for One-Way Tests in Independent Groups Designs. *R J*. 2018;10(1):175–99.
71. Noble WS. How does multiple testing correction work? *Nat Biotechnol*. 2009;27(12):1135–7.
72. Ripley B, Venables B, Bates DM, Hornik K, Gebhardt A, Firth D, et al. Package 'mass'. *Cran r*. 2013;538:113–20.
73. Csardi MG. Package 'igraph'. Last accessed. 2013;3(09):2013.
74. Barton K, Barton MK. Package 'mumin'. Version. 2015;1(18):439.
75. Gordon M, Lumley T, Gordon MM. Package 'forestplot'. Vienna: The Comprehensive R Archive Network; 2019.
76. Team RC. R: A language and environment for statistical computing (Version 4.2.2). R Foundation for Statistical Computing. 2022.
77. Li L, Victoria JG, Wang C, Jones M, Fellers GM, Kunz TH, et al. Bat guano virome: predominance of dietary viruses from insects and plants plus novel mammalian viruses. *J Virol*. 2010;84(14):6955–65.
78. Van Brussel K, Holmes EC. Zoonotic disease and virome diversity in bats. *Curr Opin Virol*. 2022;52:192–202.
79. Harvey E, Holmes EC. Diversity and evolution of the animal virome. *Nat Rev Microbiol*. 2022;20(6):321–34.
80. Huang ZY, de Boer WF, van Langevelde F, Olson V, Blackburn TM, Prins HHT. Species' life-history traits explain interspecific variation in reservoir competence: a possible mechanism underlying the dilution effect. *PLoS ONE*. 2013;8(1):e54341.
81. Huang S, Drake JM, Gittleman JL, Altizer SJE. Parasite diversity declines with host evolutionary distinctiveness: a global analysis of carnivores. *Evolution*. 2015;69(3):621–30.
82. Maganga GLD, Bourgarel M, Vallo P, Dallo TD, Ngoagouni C, Drexler JF, et al. Bat distribution size or shape as determinant of viral richness in African bats. *PLOS ONE*. 2014;9(6):e100172.
83. Perrella DF, Zima PVQ, Ribeiro-Silva L, Biagolini-Jr CH, Carmignotto AP, Galetti-Jr PM, et al. Bats as predators at the nests of tropical forest birds. *J Avian Biol*. 2019;51(1):e02277.
84. Ez CIN, Juste J, García-Mudarra JL, Agirre-Mendi PT. Bat predation on nocturnally migrating birds. *PNAS*. 2001;98(17):9700–2.
85. Nichols TA, Fischer JW, Spraker TR, Kong Q, VerCauteren KC. CWD prions remain infectious after passage through the digestive system of coyotes (*Canis latrans*). *Prion*. 2015;9(5):367–75.
86. Lee J, Malmberg JL, Wood BA, Hladky S, Troyer R, Roelke M, et al. Feline immunodeficiency virus cross-species transmission: implications for emergence of new lentiviral infections. *J Virol*. 2017;91(5):10–1128.
87. Kraberger S, Fountain-Jones NM, Gagne RB, Malmberg J, Dannemiller NG, Logan K, et al. Frequent cross-species transmissions of foamy virus between domestic and wild felids. *Virus Evol*. 2020;6(1):vez058.
88. Blackburn JK, Asher V, Stokke S, Hunter DL, Alexander KA. Dances with anthrax: wolves (*Canis lupus*) kill anthrax bacteremic plains bison (*Bison bison bison*) in southwestern Montana. *J Wildl Dis*. 2014;50(2):393–6.
89. Wrangham R, Wilson M, Hare B, Wolfe ND. Chimpanzee Predation and the Ecology of Microbial exchange. *Microb Ecol Health Dis*. 2009;12(3):186–8.
90. Malmberg JL, White LA, VandeWoude S. Bioaccumulation of pathogen exposure in top predators. *Trends Ecol Evol*. 2021;36(5):411–20.

92. Markov PV, Ghafari M, Beer M, Lythgoe K, Simmonds P, Stilianakis NI, et al. The evolution of SARS-CoV-2. *Nat Rev Microbiol*. 2023;21(6):361–79.
93. Rauw WM. Immune response from a resource allocation perspective. *Front Genet*. 2012;3:267.
94. Boggs C. Resource allocation: exploring connections between foraging and life history. *Funct Ecol*. 1992;6(5):508–18.
95. Tong S, Li Y, Rivaille P, Conrardy C, Castillo DA, Chen LM, et al. A distinct lineage of influenza A virus from bats. *PNAS*. 2012;109(11):4269–74.
96. Tong S, Zhu X, Li Y, Shi M, Zhang J, Bourgeois M, et al. New world bats harbor diverse influenza A viruses. 2013;9(10):e1003657.
97. Papkou A, Guzella T, Yang W, Koepper S, Pees B, Schalkowski R, et al. The genomic basis of Red Queen dynamics during rapid reciprocal host–pathogen coevolution. *PNAS*. 2019;116(3):923–8.
98. Kellner A, Carver S, Scorza V, McKee CD, Lappin M, Crooks KR, et al. Transmission pathways and spillover of an erythrocytic bacterial pathogen from domestic cats to wild felids. *Ecology*. 2018;8(19):9779–92.
99. Chiu ES, Kraberger S, Cunningham M, Cusack L, Roelke M, VandeWoude S. Multiple introductions of domestic cat feline leukemia virus in endangered Florida panthers. *Emerg Infect Dis*. 2019;25(1):92–101.
100. Mazzillo FF, Shapiro K, Silver MW. A new pathogen transmission mechanism in the ocean: the case of sea otter exposure to the land-parasite *Toxoplasma gondii*. *PLoS ONE*. 2013;8(12):e82477.
101. Miller MA, Miller WA, Conrad PA, James ER, Melli AC, Leutenegger CM, et al. Type X *Toxoplasma gondii* in a wild mussel and terrestrial carnivores from coastal California: new linkages between terrestrial mammals, runoff and toxoplasmosis of sea otters. *Int J Parasitol*. 2008;38(11):1319–28.

Publisher's Note

Springer Nature remains neutral with regard to jurisdictional claims in published maps and institutional affiliations.